Harvesting Energy Using a Thin Unimorph Prestressed Bender: Geometrical Effects

KARLA MOSSI,* CHRISTOPHER GREEN, ZOUBEIDA OUNAIES AND ESTHER HUGHES

Virginia Commonwealth University, 601 West Main Street, P.O. Box 843015, Richmond, Virginia 23284-3015, USA

ABSTRACT: Mathematical models and circuitry necessary for optimal energy conversion have been developed for piezoelectric devices because of their ability to convert mechanical energy to electrical energy. The piezoelectric device that is the focus of this study is a curved, thin unimorph prestressed bender. This device consists of layers of piezoelectric material, polyimide, and metal bonded at high temperatures. Effects of its layer composition and geometry on energy harvesting and actuation are investigated. Through this investigation, a method for developing empirical relationships is established and it is demonstrated that an actuator can be engineered so that the same energy output could be obtained with different materials by adjusting relevant parameters.

Key Words: energy harvesting, piezoelectricity, prestressed curved actuator, geometry effects.

INTRODUCTION

ENERGY can be reclaimed and stored for later use to recharge a battery or power a device through a process called energy harvesting. Energy harvesting, as defined by Fay and Golomb (2002), is the extraction of energy that would otherwise be wasted, from one system to power another. Some energy systems frequently wasted include solar, wind, water, indoor lighting, vibrations, acoustic noise, temperature gradients, and energy generated by humans from everyday activities such as walking, driving, or sleeping. Some of these phenomena can be harvested through the use of piezoelectric devices.

Piezoelectricity is the property of a material by which a voltage is produced as a result of a mechanical force, and conversely a mechanical deformation ensues when a voltage is applied. This property allows the material to be used as a sensor, an energy harvesting device, or an actuator. Antaki et al. (1995) explored the feasibility of extracting energy from ambulation to provide supplemental power to operate artificial organs by using PZT-based piezoelectric stacks (made from lead zirconate titanate ceramics or PZT) to measure energy used when walking or jogging. The entire device was mounted in a shoe. Although it was bulky and not practical at that point, an average power of 250–700 mW was extracted from walking, and over 2 W was obtained from jogging. Goldfarb and Jones (1999), as well as Umeda et al. (1996) measured the power and calculated the efficiency of an output produced by a piezoelectric unimorph, which consists of a layer of piezoelectric material bonded to a piece of metal. Though the efficiency obtained was quite low, their work demonstrated the possibility of using a piezoelectric device to harvest energy. Kysmissis et al. (1998) compared two piezoelectric material-based devices and a rotary magnetic generator to summarize the advantages and disadvantages as ambulatory energy harvesting mechanisms. Though the rotary magnetic generator showed a power two orders of magnitude higher than that of the piezoelectric-based devices, its implementation as an ambulatory harvesting device is difficult when compared to polyvinylidene fluoride (PVDF), and a PZT composite. Kaysap et al. (2002) utilized piezoelectric energy reclamation from strain energy induced by mechanical vibrations. In this study, 20% peak flow efficiencies were obtained with appropriate circuitry on a vibrating cantilever beam and a lumped element model is formulated to validate results. Ottman et al. (2002) proposed an energy harvesting circuit that could increase power significantly for a mechanically-excited, rectified piezoelectric device. The researchers accomplished this by developing an adaptive switching regulator that dynamically adjusts the duty cycle to maximize the output circuit. Roundy et al. (2004) developed models for different types of power converters using both electrostatic and piezoelectric conversion mechanisms validated by testing prototypes driven at vibrations similar to those found in many industrial and commercial building environments.

All studies cited above determined that the type of circuitry used to harvest energy from a piezoelectric transducer is determined by the desired output to the

*Author to whom correspondence should be addressed.
E-mail: kmmossi@vcu.edu

1045-389X/05/03 0249–13 $10.00/0 DOI: 10.1177/1045389X05050008

load, which often needs to be rectified, filtered, and regulated. In particular, Ottman et al. (2002) modeled the output signal from the transducer as an AC source in parallel with a capacitor. To convert this signal into a useful one, an AC–DC converter is used to rectify the noisy AC signal. The output from this converter is then sent to a DC–DC converter where it is regulated to the desired voltage. Capacitors are used to aid in filtering. The efficient step-down buck converter consists of a diode in series with an inductor, both in parallel with a capacitor. A microcontroller or a MOSFET controls the switching of the rectified signal. Ottman et al. further modeled the power flow characteristics of a strain-type actuator that consists of two piezoelectric layers encapsulated in a film, or a Quickpack® model QP20W from Active Control eXperts (ACX). Using this model, they determined circuitry requirements necessary for optimal power flow in order to recharge a battery. A Quickpack excited by a shaker was used in the experimental setup along with an adaptive controller, which sensed the battery current and adjusted the duty cycle to maximize current; both an AC–DC converter and a DC–DC converter were utilized. The results of this study showed that a DC–DC controller with adaptive control harvested energy at a rate four times that of direct charging without a controller. Ottman et al. (2003) expanded on their previous study by simplifying the control circuitry. They determined that a converter operating in discontinuous conduction mode would hold the optimal duty cycle close to a constant as the excitation is increased on the transducer. This approach harvested energy at three times the rate of direct charging.

Sodano et al. (2004) compared three types of strain actuators (in-plane piezoelectric patches with interdigital electrodes). In particular, a Macro Fiber Composite (MFC), a Quick Pack IDE model QP10ni, and a Quick Pack IDE model QP10n, were utilized to convert mechanical strain into electrical energy while attached to an aluminum beam. The MFC is constructed using piezoelectric PZT fibers and interdigital electrodes (IDE) as described by Williams et al. (2002). This creates an array of capacitors connected in series where the voltage adds up while the current remains constant. The Quick Pack IDE fabricated by Midé Corporation, Boston, MA, consists of four piezoelectric PZT layers embedded in a Kapton® film. Assuming that the piezoelectric materials behave as predominantly as capacitors, impedance is monitored as a function of frequency, noting that a low capacitance contributes to high impedance as shown in Equation (1),

$$Z = \frac{1}{j\omega C} \tag{1}$$

where Z is the complex impedance, ω is the input frequency, and C is the capacitance of the piezoelectric transducer. The findings of the study stress that impedance matching between the transducer and the circuit is critical when optimizing for power.

Roundy et al. (2004) have further explored the possibility of scavenging low-level vibrations as a power source for wireless sensor nodes. In this study, the geometry of the piezoelectric layer was optimized while the load resistance of the circuitry, which consisted of a series inductor with an active bridge, was varied. They modeled a PZT and PVDF bimorph, two ceramic pieces with adhesive, a generator as an AC source in series with a capacitor, and a resistor to achieve a theoretical maximum power. The model optimized mass and beam dimensions, electrode dimensions, piezoelectric thickness, steel shim thickness, and load resistance. The optimized model produced energy densities of 250 μW/cm^3 from a vibration source input magnitude of 2.5 m/s^2 at 120 Hz. The model was verified experimentally demonstrating a power density of 70 μW/cm^3. This study is one of the few that addresses both the actuator geometry and test circuitry, simultaneously.

Other types of devices studied for energy harvesting are prestressed multilayer piezoelectric composite types such as Rainbows which are chemically reduced piezoelectric wafers (Li et al., 1997); Cymbals, which consists of one layer of PZT placed between two concave metal end caps (Zhang et al., 2001); and Lipcas, which are composites of fiberglass, carbon, and PZT (Goo and Yoon, 2003). Kim et al. (2004) investigated the Cymbal transducer for energy scavenging by changing its configuration and its matching circuitry. In this study, the end-caps geometry and material were investigated with two different circuits. The first was a full-bridge rectifier with a resistive load. The second was a buck converter switched by a MOSFET. Each Cymbal was placed under load using a press and excited by a shaker. The study concluded that the higher the product of the piezoelectric field constant and the piezoelectric voltage constant, the higher the energy output.

All of the previous studies were performed on piezoelectric materials in the form of unimorph and bimorph devices, PVDF films, and stacks that utilize a vibration source for excitation. The scope of the present study focuses on one type of prestressed curved Unimorph ferroelectric driver and sensor, Thunder®, stimulated by an impulse. This device consists of a piezoelectric ceramic layer, lead zirconate titanate (PZT), and a backing metal layer, held together with a polyimide adhesive whose properties are described by Bryant (1996). After processing in an autoclave, a durable, curved, and rugged prestressed device with high out-of-plane displacement is formed, in part due to a mismatch between the coefficients of thermal expansion corresponding to the PZT and the metal layer. Several researchers have investigated this type of device and literature is widely available on its actuation and

manufacturing details: an overview of the manufacturing process of a typical device can be found in Mossi et al. (1998); an evaluation of the performance of these types of devices as compared to Rainbow actuators is presented by Wise (1998); a more detailed study on the piezoelectric properties of this device can be found in the work performed by Ounaies et al. (2001). Even though this prestressed Unimorph has been studied as an actuator for a wide range of applications, very few researchers have examined its potential as an energy conversion mechanism. Niezrecki and Balakrishnan (2001) utilized this device as an underwater propulsor; Schwartz and Narayanan (2002) enhanced its actuation performance by mechanically stressing the device; and Waterfield (2004) designed a stack of four devices of this type for a high-speed valve. As an energy harvesting device, few publications are available: Ramsay and Clark (2001) demonstrated the feasibility of utilizing the power generated in a bio-MEMS application; Mossi et al. (2001) compared different configurations of the device for actuation and energy harvesting; and Shenck and Paradiso (2001) utilized this device for harvesting energy by mounting it on a shoe.

The study presented here is designed to identify the significance of selected geometrical parameters that influence energy conversion and actuation when using a curved thin unimorph prestressed bender, or Thunder® device, designed specifically for actuation.

EXPERIMENTAL SETUP

The baseline prestressed actuator consists of a top metal layer, a piezoelectric ceramic (PZT) layer, and a metal backing layer, as shown in Figure 1. A thin layer of polyimide bonds the PZT to the top and bottom metals. The dimensions of the actuator are as follows: total length, $L = 96.52$ mm, width, $W = 71.12$ mm, and metal extension, $S = 12.7$ mm.

There are several factors that are known to influence the performance of these actuators, such as adhesive properties, metal thickness, type of metal, thickness of the piezoelectric layer, length and width of the element, driving electric fields, frequency, temperature, and boundary conditions as demonstrated by Mulling et al. (2001), Ounaies et al. (2001), and Mossi et al. (2003). The study presented here investigates the following parameters: the adhesive electrical properties of the actuator, the geometry of the device, and the type and thickness of metal backing. Each of these parameters is discussed here.

The adhesive layer used for this laminate, a soluble polyimide, is utilized in the manufacture of lightweight, adhesive-less flex circuits as shown by Holloway et al. (2002). Mossi et al. (2003) demonstrated that when this type of adhesive is utilized in the manufacturing of a Thunder® device, the voltage applied to the outside electrodes travels through the entire device thickness making the effective applied field as seen by the piezoelectric layer smaller as compared to the case when electrical leads are in direct contact with the piezoelectric layer. Direct contact leads are not available on these types of devices, yet the adhesive layer is necessary as there is evidence that it affects actuation. As such, the role of the polyimide adhesive layer for both actuation and energy scavenging is worth investigating.

Layer composition, and length-to-width ratio, have been shown to have an effect on the shape of cross-ply laminates as shown by Dano and Hyer (1998). Their study presented a methodology to predict the curvature of a laminate based on dimensionality ratios. This theory is extended to the thickness of the composites in multilayer actuators, defining a critical value of dimensionality for their optimal stable shape and actuation, as in the case of Rainbow by Li et al. (1997), and Thunder® by Hyer and Jilani (2001) and Ounaies et al. (2001). To that end, a design of experiments was performed with the objective of investigating the relevance of geometrical characteristics of the composite as it relates to energy harvesting.

The parameters to be investigated include the effect of changing the conductivity of the adhesive layer (A), the influence of the top aluminum layer (T), the effect of the ceramic layer thickness (M), the influence of the metal thickness ratio, which is defined as the metal thickness over the total device thickness (MTR), and the effect of changing the width of the device (W).

In order to evaluate the relevance of the mentioned parameters on actuation as well as on energy production,

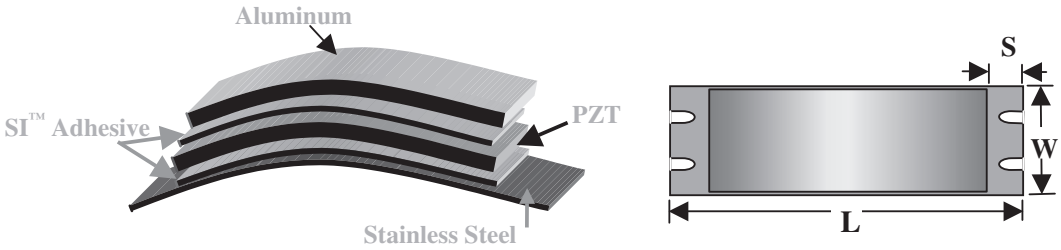

Figure 1. *Layout of a prestressed Unimorph Driver.*

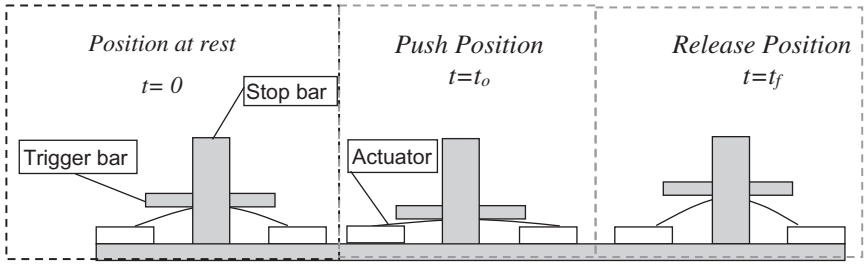

Figure 2. *Triggering mechanism.*

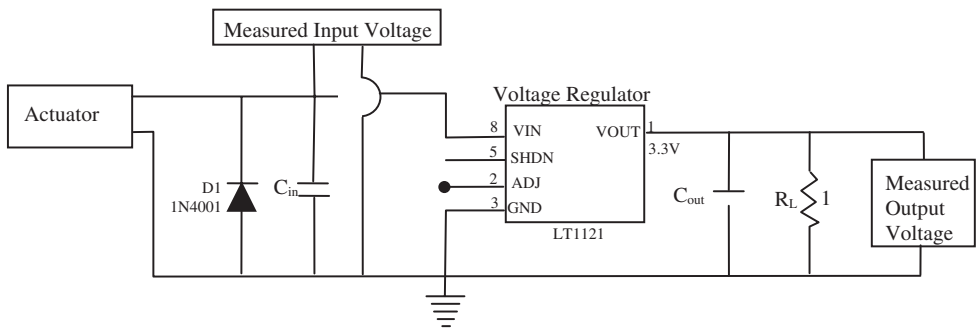

Figure 3. *Remote control circuit.*

two separate experimental setups are developed. The first setup is designed to provide relative energy measurements, performed by placing the actuator on a triggering mechanism, Figure 2. This method limits the actuator to one single stroke by controlling the boundary conditions so that a repeatable measurement can be made. The output of the transducer is then connected to a commercially available remote control switch circuitry, Figure 3. The circuit used for this study is composed of a three-stage commercial battery-less remote control. In the first stage, a diode and a capacitor are in parallel with the piezoelectric device. The diode functions as a half wave rectifier which removes the negative peaks from the signal generated by the piezoelectric device. The capacitor is used for filtering transient voltages. A low capacitance creates a high impedance hence matching the impedance of the device with the first stage of the circuit is important in cases where optimal power is a concern. In this study, however, the goal is not focused on achieving optimal power. The second stage of the circuit consists of an LT1121 voltage regulator manufactured by Linear Technology, which can regulate an input voltage ranging from 4.8 to 20 V into a 3.3 V output voltage with a supply current of up to 150 mA. The third stage of the circuit is an electrolytic capacitor and a 1 kΩ load resistor in series with the voltage regulator. The capacitor filters out transients and sets the rise time of the output signal.

Once the switch of the remote control is pressed and subsequently released, the piezoelectric device will oscillate such that there is an initial peak impulse that tapers off to infinity over time. As this initial peak can potentially destroy the voltage regulator,

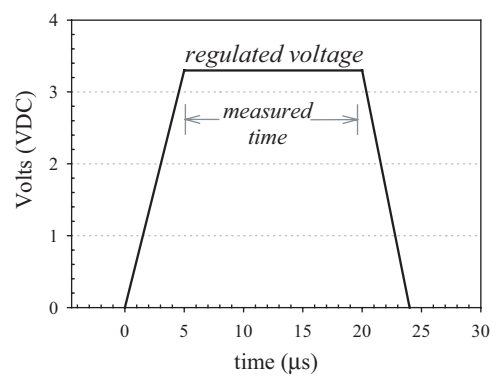

Figure 4. *Typical waveform.*

the capacitor value was changed during the experiment as a precautionary measure. The power generated from this circuit cannot be called peak or optimized power because of the relatively fixed load and line regulation of the voltage regulator. A more adequate term would be relative power due to the limitations of the circuit.

The circuit output is monitored by an oscilloscope while recording output voltage and pulse duration. A typical output waveform is shown in Figure 4. In this setup, the key factor is the length of the impulse per stroke, which is detected via the oscilloscope. The length of the stroke corresponds to the energy produced by the device and can be calculated by Equation (2) where $V = 3.3\,V_{\mathrm{rms}}$. The resistor value is kept constant at 1 kΩ, and t is the time in microseconds.

$$E = \frac{V^2}{R} \cdot t \tag{2}$$

The second experimental setup is designed to evaluate dome height and unloaded displacement performance at the geometric center of the device. Measurements are made while holding the frequency fixed at 1 Hz and varying fields with fixed and fixed–sliding boundary conditions. Along the width of the device, setscrews are used to keep the device in place, and to preserve the shape of the device along the z-axis as shown in Figure 5. The device is powered by an HP33120A signal generator, and a TREK 50/750 amplifier. Displacement and dome height are monitored at the geometric center of the device using a NAIS LM10 noncontact laser. Displacement and voltage are converted to strain and electric field, respectively. Strain is defined as the center displacement divided by the distance between electrodes, and electric field is the applied voltage divided by the distance between electrodes. For low fields, a linear slope, ΔY, is calculated with units of mm/kV. This slope is related to the piezoelectric coefficients of the PZT, and it is the parameter used when comparing the various transducer models.

A design of experimental study is employed to identify the crucial transducer parameters that affect the energy produced. Since there are multiple factors to be investigated, and main and second-order effects are more relevant, a Fractional Factorial Design is the most appropriate for this set of experiments as demonstrated by Montgomery (2001). A Full Factorial Design with 5 factors requires $2^5 = 32$ experiments, where only 5 are associated with main effects; in contrast a Fractional Factorial Design entails half of the experiments, $2^{k-1} = 2^4 = 16$ experiments. Using this model, a full experimental design is shown in Table 1.

Depending on the factor tested, two or more levels are used; for the first two experimental factors, A and T, two levels are tested (on or off); for the third experiment, the M factor, three levels of thickness are tested; for the fourth experiments, the MTR factor, two levels are tested by changing the type of metal, t_m, stainless steel and brass, with four different MTR ratios each. The last set, fifth experiment, is intended to check the effect of varying the size by changing the width, W, of the device with three different sets.

In matrix form, the experimental design can be described as Equation (3) below:

$$\begin{bmatrix} C \\ Dh \\ \Delta Y \\ E \end{bmatrix} = \begin{bmatrix} \beta_{00} & \beta_{01} & \beta_{02} & \beta_{03} & \beta_{04} \\ \beta_{10} & \beta_{11} & \beta_{12} & \beta_{13} & \beta_{14} \\ \beta_{20} & \beta_{21} & \beta_{22} & \beta_{23} & \beta_{24} \\ \beta_{30} & \beta_{31} & \beta_{32} & \beta_{33} & \beta_{34} \end{bmatrix} \cdot \begin{bmatrix} A \\ T \\ M \\ \mathrm{MTR} \\ W \end{bmatrix} + \{\varepsilon\} \tag{3}$$

where C is the capacitance of the transducer, Dh is the dome height, E is the measured energy, β_{ij} are the design parameters, and ε is the experimental error.

RESULTS

The parametric study described in the previous section is designed to investigate the relevance of geometrical parameters on energy harvesting. Results of the

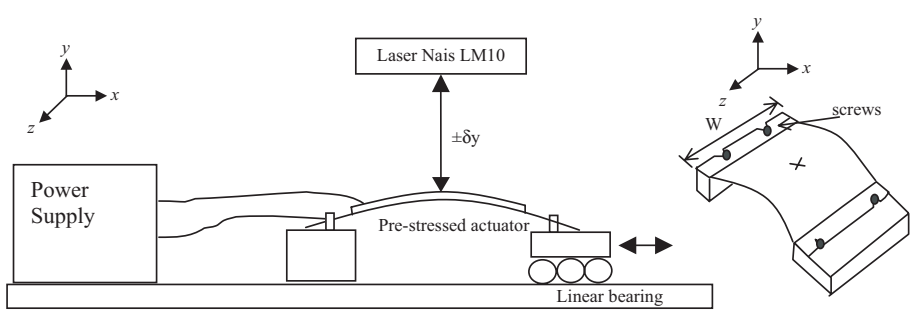

Figure 5. *Displacement experimental setup.*

Table 1. Full experimental design.

Experiment No.	Adhesive Conductivity (*A*)	Top Layer Effect (*T*)	Ceramic Thickness (*M*)	Material Thickness Ratio = M/Total Thickness (MTR)	Width (*W*)
1	On or off	Constant	Constant	Constant	Constant
2	Determined by 1A	On or off	Constant	Constant	Constant
3	Determined by 1A	Determined by 2T	Three different values	Constant	Constant
4	Determined by 1A	Determined by 2T	Determined by 3M	2 metal types, t_m, 4 different metal thickness, MTR	Constant
5	Determined by 1A	Determined by 2T	Determined by 3M	Determined by 4MTR	3 values with 2 different MTR ratios

study are divided into subsections that correspond to the experiment number described in Table 1: adhesive layer, top layer, ceramic thickness, material thickness and type, and width. A final subsection summarizes the overall effects of all of the parameters.

Adhesive Layer Effect

This experiment altered the adhesive conductivity and its impact on the measured parameters, as compared to that of a standard device. Only the bottom layer (between the PZT and the stainless steel) is made conductive, for ease of manufacturing as well as maintaining device quality, since it has been observed that the top aluminum layer, positive contact, would come in contact with the stainless steel layer, negative contact, through the top conductive layer creating a shorted device. The top aluminum layer is not smooth, in fact it is perforated during manufacturing to ensure proper adhesion, and it has a total thickness of only 0.0254 mm, the same thickness of the film used for adhesion, creating difficulties when mass manufacturing.

Experiment 1A considers the relevance of the conductivity of the adhesive layer on the four output variables of Equation (3): C, Dh, ΔY, and E. The devices consist of an aluminum top layer (0.0254 mm thick), a piezoelectric layer (0.254 mm thick), and a metal backing layer (either steel or brass, 0.2032 mm thick), all having the same width and length, namely 71.12 mm, except for the bottom metal layer which includes metal extensions, making it 96.52 mm long. The polyimide adhesive is solution-cast on a glass plate and then cured. To make the adhesive conductive, 5-μm nickel particles (at 1% weight concentration) are mixed with the polyimide-solvent solution prior to casting. The mixture is shaken using a magnetic stirrer to ensure a good dispersion of the nickel particles in the solution. Next the film is cast onto a glass surface. The film is then pulled from the plate after submerging the film in warm water. Nickel particles are selected because they are low-cost, commercially available, and suitable for increasing the conductivity of the adhesive film. The resulting film is approximately 0.0254 mm thick. Nonuniform sections are discarded. To ensure a constant adhesive thickness, an autoclave and a vacuum are applied during manufacturing of the actuator. Details on the manufacturing are discussed in a previous publication by Mossi et al. (1998). Figure 6(a) illustrates a typical nonconductive adhesive line in one of these devices, while a typical conductive (with nickel particles) adhesive line is shown in Figure 6(b).

Ten pieces of each type (conductive and nonconductive) are fabricated and an analysis of variance, or ANOVA, is employed to quantify the error and to provide an accurate measurement of the differences between the variables. Results for the 20 samples measured are shown in Table 2.

The experiments described are made under an ANOVA analysis based on the six Fisher assumptions as described by Cobb (1998): individual factors are combined by addition, unknown values are constant, average error is zero, each measurement has a standard deviation, the errors are independent, and the distribution of error follows a normal curve. The results of experiment 1A demonstrate that the changes of capacitance, C, dome-height, Dh, and displacement slope, ΔY, are not significant (p-values larger than 0.001). The analysis further shows that the energy produced, E, increases by 15.2% for the conductive case and that the changes observed on relative energy produced are significant with a p-value smaller than 0.001. The average reading for nonconductive devices is 205 μJ while for conductive devices, it is 241 μJ. Further ANOVA parameters illustrate that the observed effect on C, Dh, ΔY, and E are 99% accurate. Based on the results for Experiment 1A, all subsequent experiments are performed using a conductive adhesive although conductivity itself is not optimized and no conclusions

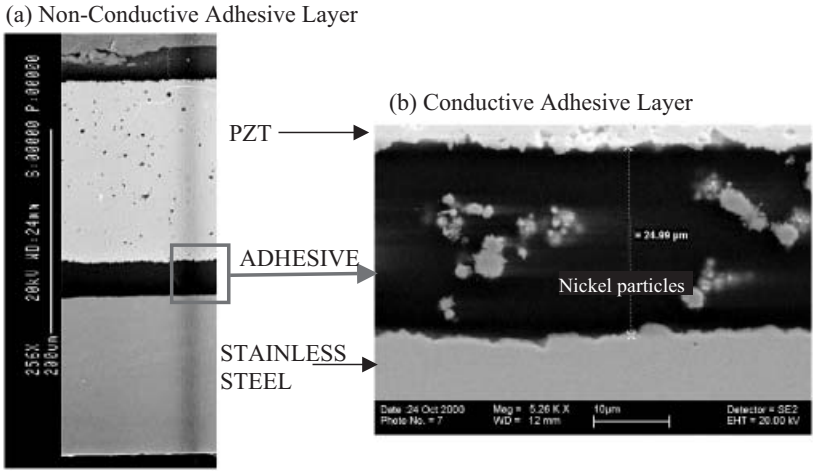

Figure 6. *Scanning electron micrograph of the adhesive layer.*

Table 2. Summary of a one-way ANOVA results.

Parameters	Capacitance (nF)		Dome Height (mm)		Displacement Slope (mm/kV)		Relative Energy (μJ)	
Groups	Nonconductive	Conductive	Nonconductive	Conductive	Nonconductive	Conductive	Nonconductive	Conductive
Average	176.4	171.8	10.58	10.94	3.25	3.02	204.64	241.19
Total degrees of freedom	19		19		19		19	
Mean squares	105.8		0.6413		0.2761		6679.2	
F	2.86		4.23		4.13		57.62	
P-value	0.1080		0.0544		0.0570		0.00000051	
Critical *F*	4.41		4.41		4.41		4.41	

can be made about the level of conductivity of the adhesive layer. To conclude this section, it is observed that conductivity, A, is a factor to be taken into account for producing more energy, yet, it is not a relevant factor when assessing C, Dh, and ΔY.

Top Layer Effect

Experiment 2T is designed to test the influence of having direct electrical contact with the PZT ceramic on all the factors mentioned earlier. Figure 6(a) shows a picture of the layer distribution on a typical device and shows that the electric field has to travel throughout the adhesive layer to make direct contact with the nickel electrodes in the piezoelectric layer. Accordingly, the transducer configurations either have a top layer (no direct contact) or no top layer (direct contact).

To ensure that the results obtained for capacitance are real, a one-way ANOVA analysis is performed in all of the chosen parameters. The results show no significant effect on dome height, Dh, with an F value smaller than F_{critical}, and p-value of 0.09 (p larger than 0.001). Results for capacitance, C, displacement slope ΔY, and relative energy output, E, are significant, that is the differences are real, with $F > F_{\text{critical}}$ and p-values of less than 0.001. Capacitance changes are expected since there is direct contact with the PZT layer. Displacement changes are also expected since the neutral axis location of the device has been altered as described by Ounaies et al. (2001). The effect of changing the location of the neutral axis is shown in Figure 7 for low-fields, with an increase in displacement slope of 33.25% from the case with a top layer.

A direct measurement of E for some of the transducers is not possible due to the limit on the maximum input voltage imposed by the regulator in the circuit. This means that the energy from transducers without a top layer and with $C < 5.6\,\mu\text{F}$ is extrapolated from other data based on a projection of the power. Using this projection, relative energy from the no-top, conductive case is 36.5% higher than the standard model (top layer, nonconductive), and 18% higher than the case with no-top and conductive adhesive. The results of this projection are shown in Figure 8, where all the linear least square regressions produced a value of R^2 higher than 92%. The error bars represent a one standard deviation scatter.

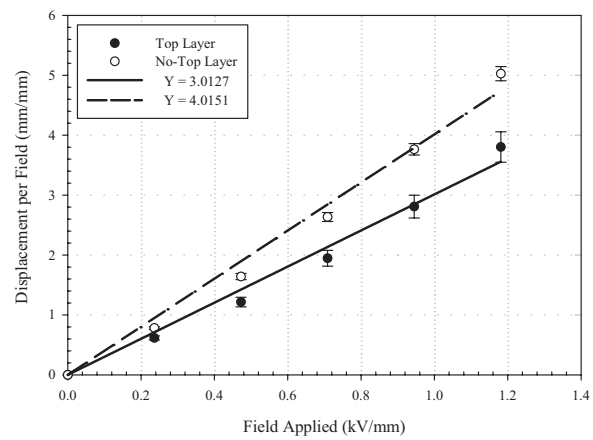

Figure 7. *Displacement slope for low electric fields.*

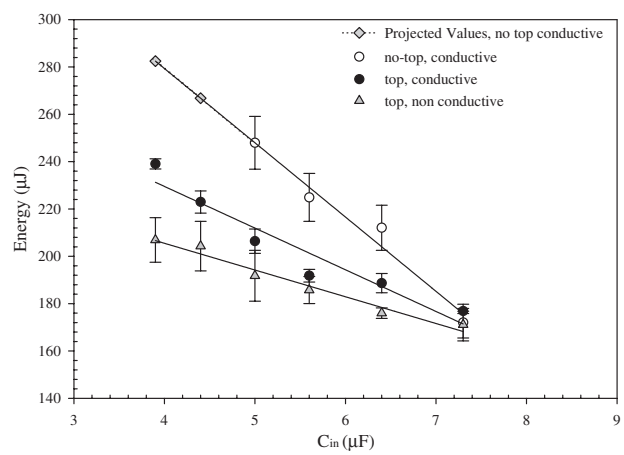

Figure 8. *Capacitor vs energy produced.*

Ceramic Thickness Effect

Experiment 3M consists of testing the ceramic thickness effect (M) by considering three ceramic

thicknesses, 0.2032, 0.2540, and 0.5080 mm. Ten actuators of each thickness were constructed with a total of 30 samples. Though this range of thicknesses is not sufficient to determine a trend, it is sufficient to determine its significance on each of the parameters evaluated. This particular range of thickness was chosen because of their availability, since deviating from standard thickness values becomes impractical and expensive. Furthermore, the objective of this stage of the experiments is to investigate the effect of changing the ceramic thickness, and not necessarily optimizing either of the parameters investigated. These actuators have characteristics that differ from the original actuator utilized, namely, they are conductive, as determined by Experiment 1A, have no-top layer, as determined by Experiment 2T, and have the same metal thickness and width as the one used in Experiments 1A and 2T.

With emphasis on the effect of thickness changes, a one-way ANOVA analysis is performed in all the measurements. All the parameters in this case showed significant differences according to the ANOVA analysis, with an increase in energy production of 45% in Experiment 1A and 25.5% in Experiment 2T when a ceramic thickness $M = 0.2540$ mm is selected. These results are based on an exploratory design between factors, which is performed by plotting each factor and their variation with M, as shown in Figure 9(a)–(d). This method qualitatively identifies trend variations and the relationships among factors – that is the independent variables and the dependent variables. Analyzing the trends, it can be observed that C and ΔY show the same behavior, perhaps due to their dependence on materials properties (such as dielectric constant and piezoelectric strain coefficients). Dome height, Dh, and energy, E, also follow a similar trend, peaking to an optimum value for both Dh and E.

Although 30 samples were measured, this experiment shows that the results are affected only by changing ceramic thickness. For convenience, only one value of ceramic thickness is chosen for the next stage.

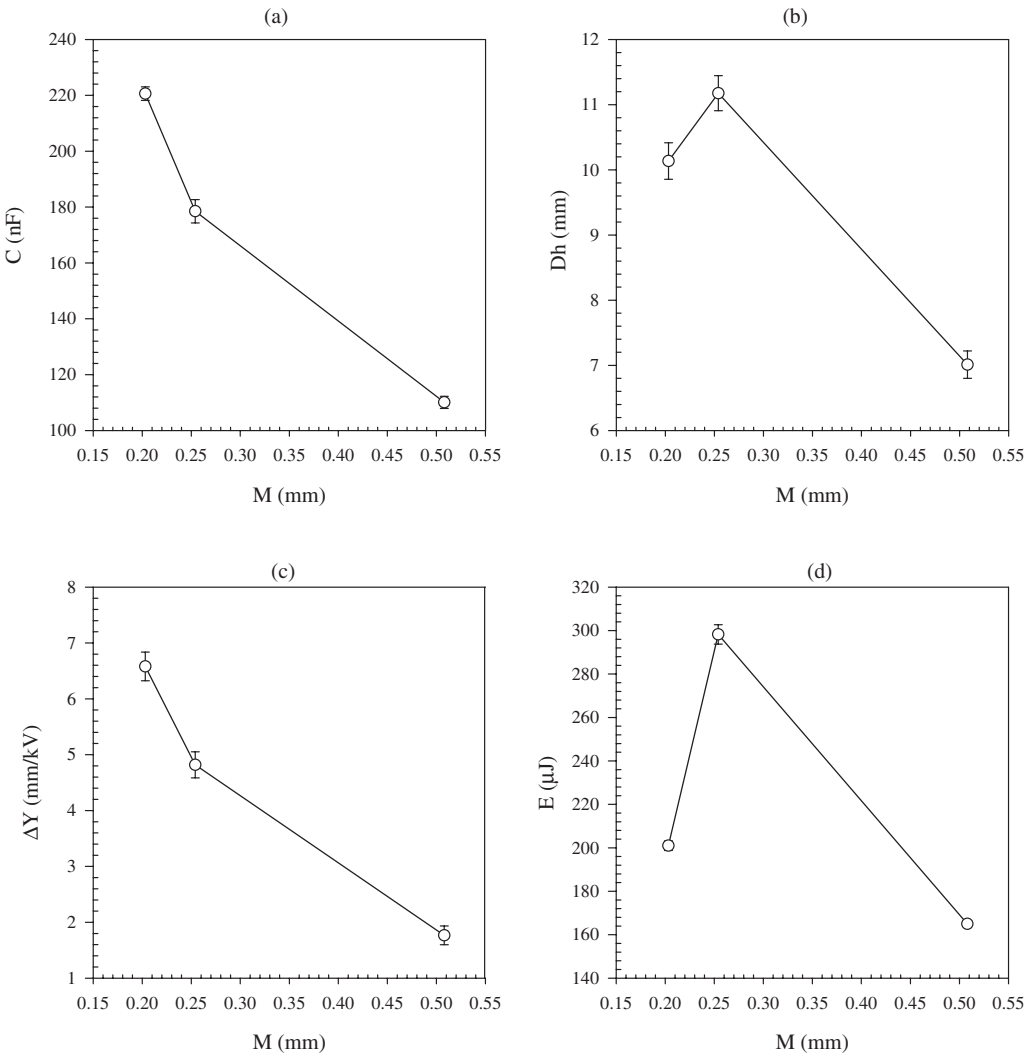

Figure 9. *Variation of Y parameters with M.*

To completely identify this effect, a numerical simulation may be necessary. At this stage, the best energy-harvesting device is composed of a conductive adhesive layer (A), no-top layer (T), and a 0.2540 mm ceramic layer (M).

Metal Thickness and Type Effect

Experiment 4MTR aims to assess the effect of MTR, metal thickness, and metal type, t_m, on C, Dh, ΔY, and E. This is accomplished by keeping the ceramic thickness constant at 0.2032 mm and varying the metal thickness, (0.1524, 0.2032, 0.254, and 0.3048 mm) using both stainless steel and brass bottom layers. A total of 80 pieces were tested in this experimental phase, 10 pieces per type of metal, and four different thicknesses per metal type. It is noted that the ceramic thickness used for experiment 3M is not the best in terms of producing the highest energy. This is attributed to the limitations on the circuitry utilized in this study.

To illustrate the influence of the parameter MTR, Figures 10 and 11 are shown for stainless steel and brass, respectively where MTR versus displacement and dome height are shown. Note that MTR can include both metals as shown in Figure 12 showing maximum displacement only. Since MTR seems to play an important role in displacement, it needs to be taken into account as a factor for energy.

The interaction between parameters can be investigated by performing a two-way analysis of variation with interaction, or two-way ANOVA, for all of the factors. In short, this interaction is represented by Equation (4) where y represents C, Dh, ΔY, and E; μ represents the grand average for each of the values for y; α represents the type of metal; β represents the metal thickness, ($\alpha\beta$) represents the interaction between type and metal thickness, and e represents the residual error. The subscript i represents the first factor metal type, $\alpha_1 =$ stainless steel, and $\alpha_2 =$ yellow brass; subscript j represents the second factor metal thickness,

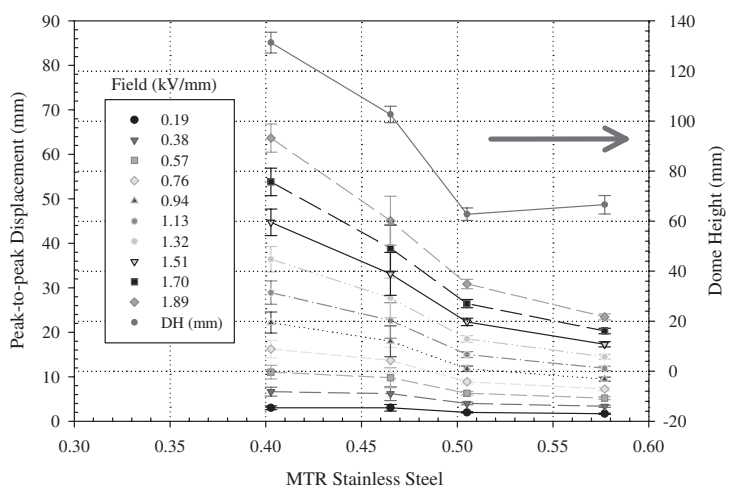

Figure 10. *MTR for steel vs displacement and dome height.*

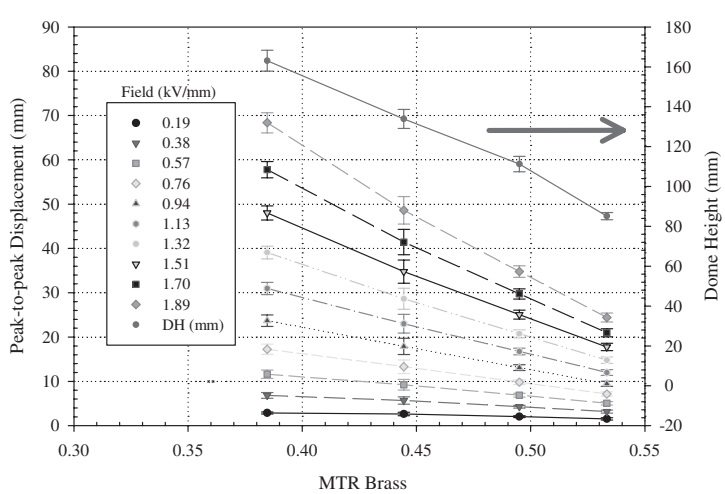

Figure 11. *MTR for brass vs displacement and dome height.*

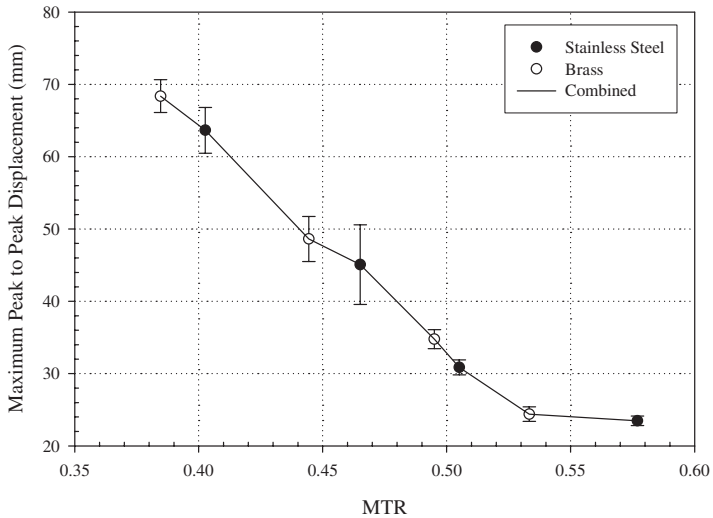

Figure 12. *MTR and maximum displacement*

Table 3. Summary of two-way ANOVA.

	Summary of ANOVA Parameters	Capacitance (nF)	Dome Height (mm)	Displacement Slope (mm/kV)	Relative Energy (μJ)
α	Degrees of freedom	79	79	7	79
	F	170.917	1411.378	0.991	9356.583
	P-value	1.15E − 32	4.80E − 49	0.393	5.72E − 78
	$F_{critical}$	2.732	3.974	10.128	3.974
β	Degrees of freedom	79	79	7	79
	F	0.004	1418.275	149.841	10039.204
	P-value	0.951	6.21E − 64	9.15E − 04	2.65E − 94
	$F_{critical}$	3.974	2.732	9.277	2.732
$(\alpha\beta)$	Degrees of freedom	79	79	–	79
	F	9.277	52.307	–	2945.309
	P-value	2.90E − 05	4.69E − 18	–	3.20E − 75
	$F_{critical}$	2.732	2.732	–	2.732

β_{i1} =0.1524 mm, β_{i2} = 0.2032 mm, β_{i3} = 0.2542 mm, β_{i4} = 0.3048 mm; and k varies from 1 to 10 which corresponds to the number of samples measured.

$$y_{ijk} = \mu + \alpha_i + \beta_j + (\alpha\beta)_{ij} + e_{ijk} \tag{4}$$

The results for the two-way ANOVA, Table 3, shows that differences obtained by varying type of metal, α, in the displacement slope at low fields, ΔY, are not real since the p-value for displacement slope is greater than 0.001; however, the differences are real for all other parameters, p-values less than 0.001. The differences between metal thickness, β, are relevant for the parameters, Dh, ΔY, and E with p-values smaller than 0.001. For C, the differences in metal thickness are irrelevant.

Width Effect

Experiment 5W, consisted of changing the variable W using two sets of MTR values since it was shown that the MTR variable plays a key role in the previous set of experiments. By performing the same type of analysis, it is found that the changes in width are only relevant for C, capacitance, and E, energy (p-value less than 0.001). Summarizing the results from all five experiments, Equation (2) becomes Equation (5) where k represents a constant value.

$$\begin{bmatrix} C \\ Dh \\ \Delta Y \\ E \end{bmatrix} = \begin{bmatrix} k & k & k & \beta_{03} & \beta_{04} \\ k & k & k & \beta_{13} & \beta_{14} \\ k & k & k & \beta_{23} & \beta_{24} \\ k & k & k & \beta_{33} & \beta_{34} \end{bmatrix} \cdot \begin{bmatrix} A \\ T \\ M \\ \mathrm{MTR} \\ W \end{bmatrix} + \begin{bmatrix} \varepsilon_1 \\ \varepsilon_2 \\ \varepsilon_3 \\ \varepsilon_4 \end{bmatrix} \tag{5}$$

Performing multilinear regressions, such as to identify beta β_{i4} in Equation (5), keeping A, T, and M constant, the results indicate that the parameters β_{04}, β_{14}, β_{34} cannot be determined because the multilinear regression shows that the probability of the parameters or the p-value, is very large and therefore has no significance on the model and a different model may be better suited.

Discussion of Overall Effects

Each previous section systematically evaluates the significance of parameters, relevant for actuation, on energy harvesting. Since the objective of this study is to identify the relevant geometrical parameters that have a significant effect on energy, identifying an expression for E can be derived for this specific circuit and device. Results can be represented by a new set of equations that show the parameters that are statistically significant for each of the measured parameters in Equations (6)–(9).

$$C = C(T, M, t_m, W) \tag{6}$$

$$Dh = Dh(M, t_m, \mathrm{MTR}) \tag{7}$$

$$\Delta Y = \Delta Y(T, M, \mathrm{MTR}) \tag{8}$$

$$E = E(A, T, M, t_m, \mathrm{MTR}, W) \tag{9}$$

From the previous equations, expressions represented by Equations (7) and (8) have the least number of variables and are therefore simpler to analyze. Dome height, Equation (7), is a function of M and MTR, and t_m. Hence a multilinear regression approach of the form shown in Equation (4) can be performed, see Equation (10). Note that t_m indicates type of metal, and the parameter to represent the type of metal can be a measure of the mechanical properties, such as Young's modulus, the coefficient of thermal expansion, or Poisson's ratio.

$$Dh = x_3 \cdot M + x_4 \cdot \mathrm{MTR} + x_5 \cdot t_m + \varepsilon \tag{10}$$

The results by using the modulus of elasticity of the two metals utilized, stainless steel type 302, ASTM A666, full hard, 195 GPa, and Yellow Brass, ASTM B19, B36, half-hard, 100–110 GPa, show that x_5 is not a significant parameter in the equation (p-value for t_m is 0.7). Other material properties or combination of properties maybe more relevant and are not evaluated in this expression. By utilizing x_3 and x_4, in the regression only, the results show that $x_3 = -46.51$, $x_4 = 47.32$, and $\varepsilon = 0$ with an R-value of 75% which indicates that Dh is a factor that depends not only on M and MTR but on other parameters, different from modulus of elasticity, not taken into account in this study. To model dome height, material properties such as Young's modulus and coefficient of thermal expansion are important. Mathematical models including all the relevant parameters have been developed by Capozzoli et al. (1999), and Ochinero and Hyer (2002).

To obtain a general expression for ΔY, a multilinear regression of Equation (8) becomes of the form of Equation (11), eliminating the effect of the top layer, since only one variation was made for that case.

$$\Delta Y = x_1 \cdot M + x_2 \cdot t_m + \varepsilon \tag{11}$$

where $x_1 = -33.59$, $x_2 = 17.36$, $\varepsilon = 18.06$ with an R-value of 96%. This equation is valid for low fields, with ΔY in units of mm/kV. One of the limitations of these equations is that the data utilized for this regression does not represent all of the possible combinations that a device can have, such as metal thickness ranges, which were very limited in this study.

Taking into consideration that Dh is a function of M and MTR, the relevant variables for dome height, then for the expression for energy, Equation (9), can be reduced by substituting M and MTR for Dh. Since there is an insufficient number of variations for the variables A, conductivity, and T, top layer effect, then the expression for energy can be reduced to form an expression of the form shown in Equation (12) with only the variables Dh, and W.

$$E = x_5 \cdot Dh + x_6 \cdot W + \varepsilon \tag{12}$$

where $x_5 = 16.03$, $x_6 = 7.39$, $\varepsilon = -472.06$, and $R = 93\%$. It is important to note that a device with zero dome height, $Dh = 0$, can produce energy as well, as in the case of a device fabricated with materials such as carbon and fiberglass, such as the Lipca devices described by Goo and Yoon (2003). A summary of the results predicted by Equation (12) is shown in Figure 13 for constant values of W.

The previous equations constitute empirical relationships and are only valid for elements of the length used for this study, $L = 96.72$ mm including metal extensions. This expression cannot be used for optimizing energy of a prestressed piezoelectric actuator. However, it illustrates the methodology to eliminate, and combine the relevant variables related to the geometry of the actuator into a model where optimization can be performed. Further development into the modeling aspects of this device will provide a clearer picture of the mechanisms that govern the behavior of these devices.

CONCLUSIONS

An investigation of parameters that affect actuation (quantified by ΔY) and energy harvesting (E) is performed on a standard prestressed piezoelectric actuator. Parameters such as conductivity of the adhesive, composition, size, and type and thickness of the layers, are investigated using a fractional factorial experimental design. Statistical analyses of all the results are performed to determine the significance of the parameters tested on the factors of interest, mainly displacement and energy production. It is shown that conductivity of the adhesive improves energy conversion capabilities but has no effect on displacement, noting that the level of conductivity itself is not optimized. The composition of the layers is shown to have a strong influence on both actuation and energy conversion.

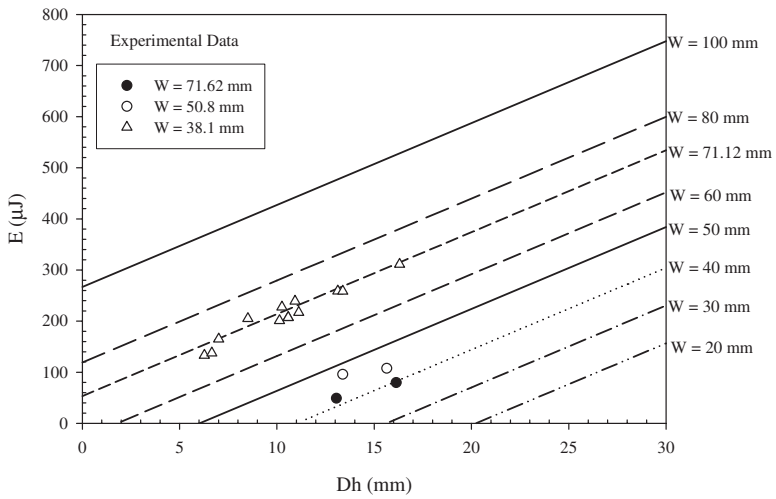

Figure 13. *Energy predictions vs dome height*

Metal type alone, however, does not show a significant influence on either actuation or energy conversion. Metal thickness, metal type, and metal ratio, MTR, combined have a significant influence on dome height, most likely because these parameters have a role in predicting the geometry of the device as shown by the models developed by Capozzoli et al. (1999) and Ochinero and Hyer (2002). Dome height is shown to be significant for energy harvesting, but not for displacement at low-fields. Displacement at low-fields is shown to be a function of ceramic thickness, M, and metal thickness, t_m, but not on MTR or dome height, Dh, indicating that another parameter not investigated in this work maybe more suitable for characterizing the displacement of this type of device. It is also demonstrated that geometrical factors affect energy conversion. These facts are clearly illustrated by the 45% improvement in energy conversion capabilities accomplished with no-top layer, a conductive adhesive, and the appropriate geometry of the layers. Finally, a method for developing empirical relationships is established and it is demonstrated that an actuator can be engineered so that the same energy output could be obtained with different materials by adjusting relevant geometrical parameters. Hence, the device can be designed to meet space requirements.

ACKNOWLEDGMENTS

The authors are grateful for the kind support provided by Face International Corporation, Norfolk, VA, USA.

REFERENCES

Antaki, J., Bertocci, G., Green, E., Nadeem, A., Rintoul, T., Kormos, R. and Griffith, B. 1995. "A Gait Powered Autologous Battery Charging System for Artificial Organs," *ASAIO Journal*, 41:M588–M595.

Bryant, R. 1996. "LaRC™-SI: A Soluble Aromatic Polyimide," *High Performance Polymers*, 8:607–615.

Capozzoli, M., Gopalakrishnan, J., Hogan, K., Massad, J., Tokarchik, T., Wilmarth, S., Banks, H., Mossi, K. and Smith, R. 1999. "Modeling Aspects Concerning Thunder Actuators," *Proc. SPIE Int. Soc. Opt. Eng.*, 3667:719–727.

Cobb, G. 1998. *Introduction to Design and Analysis of Experiments*, Springer-Verlag, New York, NY.

Dano, M.L. and Hyer, M.W. 1998. "Thermally-induced deformation behavior of unsymmetric laminates," *Intl. Journal of Solids and Structures*, 35(17):2101–2120.

Fay, J. and Golomb, D. 2002. *Energy and the Environment*, Oxford University Press, New York, NY.

Goldfarb, M. and Jones, L. 1999. "On the Efficiency of Electric Power Generation with Piezoelectric Ceramic," *Journal of Dynamic Systems, Measurement, and Control*, 121:566–571.

Goo, N. and Yoon, K. 2003. "Analysis of Lipca-C Actuators." *International Journal of Modern Physics*, B17(8 & 9):1959–1964.

Holloway, N., Barnes, K., Draughon, G. and Scott, L. 2002. "Fabrication of Adhesiveless Lightweight Flexible Circuits Using Langley Research Center Solubleimide LaRC SI Polyimide Film," *Proc. SPIE Int. Soc. Opt. Eng.*, 4698:293–303.

Hyer, M.W. and Jilani, A.B. 2001. "Manufactured shapes of rectangular RAINBOW actuators," *42nd AIAA/ASME/ASCE/AHS/ASC Structures, Structural Dynamics, and Materials Conference*, 4:2824–2834.

Kaysap, A., Lim, J., Johnson, D., Horowitz, S., Nishida, T., Ngo, K., Sheplak, M. and Cattafesta, L. 2002. "Energy Reclamation from a Vibrating Piezoceramic Composite Beam," In: *9th International Congress on Sound and Vibration*, ICSV9.

Kim, H., Batra, A., Priya, S., Uchino, K., Newnham, R. and Hoffman, H. 2004. "Energy Harvesting Using A Piezoelectric Cymbal Transducer in Dynamic Environment," *Actuator 2004, 9th International Conf. on New Actuators Proc.*, P119:812–816.

Kymissis, J., Kendall, C., Paradiso, J. and Gershenfeld, N. 1998. "Parasitic Power Harvesting in Shoes," In: *Second IEEE International Conference on Wearable Computing (ISWC)*, IEEE Computer Society Press, pp. 132–139.

Li, G., Furman, E. and Haertling, G. 1997. "Stress Enhanced Displacements in PLZT Rainbow Actuators," *American Ceramic Society*, 80(6):1382–1388.

Montgomery, D. 2001. *Design and Analysis of Experiments*, 5th edn, John Wiley and Sons, New York, NY.

Mossi, K., Ounaies, Z. and Oakley, S. 2001. "Optimizing Energy Harvesting of a Composite Unimorph Pre-stressed Bender," In:

16th Technical Conference of the American Society for Composites, September 9–12, Blacksburg, VA.

Mossi, K., Ounaies, Z., Smith, R. and Ball, B. 2003. "Prestressed Curved Actuators: Characterization and Modeling of their Piezoelectric Behavior," *Proc. SPIE Int. Soc. Opt.*, 5053:423–435.

Mossi, K., Selby, G. and Bryant, R. 1998. "Thin-layer Composite Unimorph Ferroelectric Driver and Sensor Properties," *Materials Letters*, 35:39–49.

Mulling, J., Usher, T., Dessent, B., Palmer, J., Franzon, P., Grant, E. and Kingon, A. 2001. "Load Characterization of High Displacement Piezoelectric Actuators with Various End Conditions," *Sensors and Actuators A: Physical*, 94:19–24.

Niezrecki, C. and Balakrishnan, S. 2001. "Power Characterization of THUNDER Actuators as Underwater Propulsors," *Proc. SPIE Int. Soc. Opt.*, 4327:88–98.

Ochinero, T. and Hyer, M. 2002. "Manufacturing Distortions of Curved Composite Panels," *Journal of Thermoplastic Composite Materials*, 15(2):79–87.

Ottman, G., Hoffman and Lesieutre, G. 2003. "Optimized Piezoelectric Energy Harvesting Circuit Using Step-Down Convertor in Discontinuous Conduction Mode," *IEEE*, 18(2):696–703.

Ottman, G., Hoffman, H., Bhatt, A. and Lesieutre, G. 2002. "Adaptive Piezoelectric Energy Harvesting Circuit for Wireless Remote Power Supply," *IEEE Transactions On Power Electronics*, 17(5):669–676.

Ounaies, Z., Mossi, K., Smith, R. and Berndt, J. 2001. "Low-field and High Field Characterization of Thunder Actuators," *Proc. SPIE Int. Soc. Opt*, 4333:339–407.

Ramsay, M. and Clark, W. 2001. "Piezoelectric Energy Harvesting for Bio MEMS Applications," *Proc. SPIE Int. Soc. Opt. Eng.*, 4332:429–438.

Roundy, S., Wright, P. and Rabaey, J. 2004. *Energy Scavenging For Wireless Sensor Networks*, Kluwer Academic Publishers, New York, NY.

Schwartz, R. and Narayanan, M. 2002. "Development of High Performance Stress-biased Actuators through the Incorporation of Mechanical Pre-loads," *Sensors and Actuators A: Physical*, 101(3):322–331.

Shenck, N. and Paradiso, J. 2001. "Energy Scavenging with Shoe-mounted Piezoelectrics," *IEEE Micro*, 21(i3):30–43.

Sodano, H., Lloyd, J. and Inman, D. 2004. "An Experimental Comparison Between Several Active Composite Actuators For Power Generation," *Proc. SPIE Int. Soc. Opt. Eng.*, 5390:370–378.

Umeda, M., Nakamura, K. and Ueda, S. 1996. "Analysis of the Transformation of Mechanical Energy to Electrical Energy Using Piezoelectric Vibrator," *Japanese Journal of Applied Physics – Part 1 Regular Papers and Short Notes*, 35(5B):3267–3274.

Waterfield, G. 2004. "High Performance Pre-stressed Piezoelectric Bender Actuator for Digital Valves," *Ceramic Transactions*, 150:467–482.

Williams, R., Grimsley, B., Inman, D. and Wilkie, W. 2002. "Manufacturing and Mechanics-based Characterization of Macro Fiber Composite Actuators," *ASME Aerosp. Div. Publ. AD*, 67:79–89.

Wise, S. 1998. "Displacement Properties of RAINBOW and THUNDER Piezoelectric Actuators," *Sensors and Actuators A*, 69(1):33–38.

Zhang, J., Hladky-Hennion, A., Hughes, W. and Newnham, R. 2001. "Modeling and Underwater Characterization of Cymbal Transducers and Arrays," *IEEE Transactions on Ultrasonics, Ferroelectrics, and Frequency Control*, 48(2):560–568.